FEASIBILITY OF IN VIVO MR IMAGE-BASED MICRO FINITE-ELEMENT ANALYSIS OF THE PROXIMAL FEMUR

Maite Aznarez-Sanado[1], Chamith S Rajapakse[1], Ning Zhang[1], Jeremy F Magland[1], Michael J Wald[1], Alex C Wright[1], Yusuf A Bhagat[1], Wenli Sun[1], and Felix W Wehrli[1]

[1]*Laboratory for Structural NMR Imaging, University of Pennsylvania, Philadelphia, Pennsylvania, United States*

INTRODUCTION

Proximal femur fractures are common in the older population and are known to result in high rates of mortality. Therefore, assessment of fracture risk at the proximal femur on the basis of *in vivo* images would be of considerable clinical interest. Micro Finite-Element Analysis (μFEA) is a promising tool for the assessment of bone strength and fracture risk [1-2]. Owing to its accuracy in resolving bone micro-architecture, high-resolution (10-50μm) micro-computed tomography (μCT) performed in cadaveric bone specimens is considered the gold standard for the generation of μFE models of trabecular bone (TB). Acquiring *in vivo* micro magnetic resonance images (μMRI) at the proximal femur is challenging due to SNR constraints at this anatomic location. Recent advances in MRI allow acquisition of *in vivo* images of the proximal femur at improved resolution (e.g., 240μm in plane and 500-1000μm through plane voxel sizes [3-4]). The main goal of the present study was to examine the feasibility of μFEA on the basis of *in vivo* μMR images of the proximal femur. Toward this goal, strain maps derived from μCT and simulated μMR images at *in vivo* resolution were qualitatively compared to data derived from an *in vivo* μMR image.

METHODS

***In vivo* μMR acquisition**: One subject (male, 38 years old) was scanned at 3T (Siemens TIM Trio) using the manufacturer's Spine and Body Matrix coils. High-resolution images of the proximal femur were acquired using a modified 3D Fast Large-Angle Spin Echo (FLASE) sequence [5]. Sequence parameters were: TR=80ms, TE=11ms, flip angle=150°, FOV=153.6x219x13mm^3, matrix size=512x730x24, giving a voxel size of 300μm^2 in the oblique coronal plane and 550μm through plane. The bone was segmented manually from soft tissue at the periosteum boundary. The grayscale MR image intensities were normalized to the mean signal values of pure "marrow", with pure bone and pure "marrow" having minimum and maximum values. Subsequently, contrast of the resulting images was inverted to generate bone-volume fraction (BVF) maps, in which bone appears hyperintense.

***Ex vivo* μCT acquisition**: The proximal end of an intact human femur, with marrow *in situ*, from an 87-year old female donor was imaged by micro-CT (X5000, North Star Imaging Rogers, MN) and reconstructed at 45μm isotropic voxel size (efX-CT, North Star Imaging). Due to computer memory constraints the original μCT data were downsampled to 80μm isotropic voxel size to yield gray-scale BVF maps that served as input into the μFE model. To generate simulated μMRI data at *in vivo* imaging resolution (315x315μm^2 in coronal plane, 500μm through plane), the original μCT data was first binarized and then intensity inverted. This image was then converted to k-space by Fast Fourier Transform and low-pass filtered with a 3D rectangular function to achieve the desired resolution. In addition, Gaussian noise was added to yield a magnitude "μMRI" data set with SNR~10 and a BVF map was generated following the procedure described earlier.

μFE-model generation: μFEA was performed for each of the BVF maps derived from the high-resolution μCT data, the simulated μMRI dataset and the *in vivo* μMR images. First, each bone voxel in the BVF map was directly transformed to a hexahedral finite element with dimensions equal to the voxel size. Bone tissue was assumed to be isotropic and linearly elastic. Each element's Young's modulus (YM) was set proportional to BVF at that voxel, i.e. YM = (15 GPa) × (BVF). Poisson's ratio was kept constant at 0.3. Compressive loading was simulated along the inferosuperior direction by applying a constant vertical displacement (~1% strain) to all FE nodes in contact with the acetabulum of the pelvis while keeping those in the distal face constrained. The μFE simulations yielded 3D strain maps corresponding to the femoral volume. Since the load was applied along the inferosuperior axis, the generated strain maps represented the stance-phase loading.

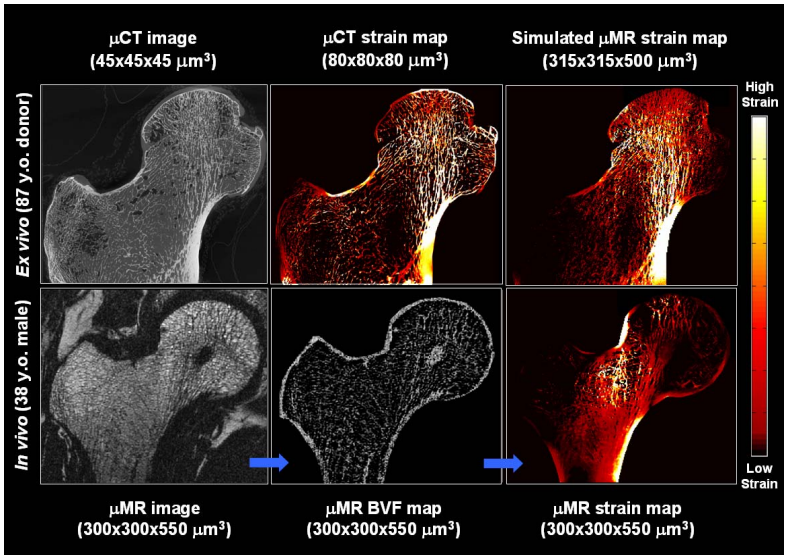

Figure. *Strain maps corresponding to the stance-phase loading obtained for each data set.* ***Upper row:*** *High-resolution μCT image and corresponding strain maps derived at different resolutions and noise levels.* ***Lower row:*** *Processing steps necessary for obtaining the strain map related to the in vivo μMR image acquisition (blue arrows).*

RESULTS AND DISCUSSION

The three data sets show similar loading characteristics (see Figure). In all the cases, the load was transferred from the femoral head to the medial cortex through the trabecular bone, in agreement with previous μCT studies [6]. The similarity in the 3D distribution of strain obtained for high-resolution data with those generated at lower resolution as well as for *in vivo* μMR images suggests that μFEA may be feasible in the *in vivo* regime of limited spatial resolution and SNR. The present data are further supported by the strong correlation (R^2=0.99) and slope close to unity found by the authors between derived μFE-mechanical parameters from high resolution (45μm μCT data set) and simulated μMR images (270x500x270μm^3 voxel size, SNR~10) [7]. The present work is the first showing strain maps derived from an *in vivo* μMR image at the proximal femur. One of the main limitations of this study is that the *in vivo* MR acquisition did not cover the entire volume of the proximal femur. Implementation of parallel imaging methods to the current imaging protocol should enable acquisition of a volume encompassing the entire hip in a clinically practical scan time.

CONCLUSION

The current results indicate the feasibility of μFEA performed on the basis of *in vivo* μMR images of the proximal femur.

ACKNOWLEDGEMENTS NIH grants RO1 AR55647, RO1 AR53156 and K25 AR 060283

REFERENCES [1] Boutroy et al, JBMR, 2008 [2] Vilayphiou, Bone, 2010 [3] Krug, Radiol Clin North Am., 2010 [4] Folkesson, Bone, 2011 [5] Magland et al, MRM, 2009 [6] Van Rietbergen, JBMR, 2003 [7] Aznarez-Sanado et al, ORS, 2012.